Artical ID:1006-3471(2012)06-0548-18

Electrochemical Performance of Screen-Printed Composite Coatings of Conducting Polymers and Carbon Nanotubes on Titanium Bipolar Plates in Aqueous Asymmetrical Supercapacitors

Xiaohang Zhou, George Z. Chen*

(*Department of Chemical and Environmental Engineering, and Energy and Sustainability Research Division, Faculty of Engineering, University of Nottingham, Nottingham NG7 2RD, UK*)

Abstract: Composites of conducting polymers (polypyrrole and polyaniline) with acid treated multi-walled carbon nanotubes were formulated into printable aqueous inks, with the aid of functional additives (benzethonium chloride as a surfactant with or without polyvinyl alcohol as a binder). The inks were screen-printed as fairly uniform coatings of various mass loading densities and areas (up to 75 mg·cm^{-2} and 100 cm^2) on thin titanium plates (0.1 mm in thickness). These screen-printed plates were used to fabricate both unit cell and multi-cell stack of asymmetrical supercapacitors with screen-printed negative electrodes of activated carbon (pigment black) in aqueous electrolytes (3.0 mol·L^{-1} KCl or 1.0 mol·L^{-1} HCl). In particular, a three-cell stack with two bipolar Ti plates of 100 cm^2 in screen-printed area was constructed, demonstrating promising technical specifications: 3.0 V in stack voltage, 1.29 ~ 1.83 F·cm^{-2} in electrode capacitance, 2.30 ~ 3.24 Wh·kg^{-1} in specific energy, and 1.04 kW·kg^{-1} in maximum specific power. Cyclic voltammetry, galvanostatic charging and discharging, and electrochemical impedance spectrometry were applied to study the composites, screen-printed coatings and individual and bipolarly stacked cells, assisted by optical and electron microscopy.

Key words: screen-printing; supercapacitors; conducting polymers; carbon nanotubes; bipolar plates; titanium

CLC Number: O646; TM53 **Document Code:** A

1 Introduction

Supercapacitors, also known as electrochemical capacitors, are an important development in the field of energy storage and conversion[1-2]. They show ultra large specific capacitance, store electric charge in a highly reversible way, as a conventional capacitor does, and operate at very large specific power, e.g. 100 kW·kg^{-1}, whilst common batteries can rarely export beyond 1.0 kW·kg^{-1}.

In supercapacitors, charge storage can occur through either or both of two mechanisms[2]. The first mechanism is related with, for example, specially processed carbons that have large specific surface areas and, when in contact with an electrolyte, offer much higher interfacial charge storage capacity than the dielectric materials in conventional capacitors. The charge stored at the carbon/electrolyte interface, which is effectively an electric double layer, can be discharged very fast (in seconds to minutes), giving rise to high pulsed power. The charging and discharging proceed through electrostatic interaction, involving no chemical reaction. Early supercapacitors were mostly made from various activated carbons because of their high specific surface areas and low costs. The specific surface areas of activated carbons range from 500 to 3000 m^2·g^{-1}, arising from a complicated arrangement of internal pores. However, full utilisation of the high surface area of

Received: 2012-05-15, Revised: 2012-08-31 *Corresponding author, Tel: +44 115 9514171, Fax: +44 119 9514115, E-mail: george.chen@nottingham.ac.uk

The authors thank E.ON AG for funding through the E.ON International Research Initiative-Energy Storage 2007.

activated carbons is never achieved for various reasons [3-6]. Also, porous carbons are generally low in conductivity, which compromises the power capability. More advanced carbons, such as carbon nanotubes (CNTs) and graphenes, have been studied for supercapacitor applications[7-8]. They can offer higher conductivities, but show smaller specific capacitance compared with activated carbons.

The second charge storage mechanism is present in the so called pseudocapacitors which use redox active materials, such as transition metal oxides (TMOs) and electronically conducting polymers (ECPs), as the electrode materials. Charge storage in pseudocapacitors occurs through redox reactions not only at the electrode/electrolyte interface, but also within the electrode materials. Such redox reaction based charge storage (pseudocapacitance), also known as Faradaic storage, is thus much higher in capacity than the electrostatic interaction based charge storage in electric double layer capacitors. However, the charge storage in TMOs or ECPs suffers from microscopic stress cycles due to intercalation and depletion of the charge balancing ions, and the relatively low electron and ion conductivities, leading to lower stabilities and power[9-11].

To overcome the drawbacks of the above mentioned double layer capacitance and pseudo-capacitance materials, composites such as that of ECPs and carbon nanotubes (CNTs) have been developed in the past decade, showing many improved properties for supercapacitor applications[8,12-13]. More recently, an ECP-CNT composite was applied in a 20 V stack of bipolarly connected supercapacitors [12]. Such a multi-cell stack uses fewer current collectors than those in individual cells externally connected to achieve the same overall working voltage, and hence have higher energy capacity and power capability if normalised to the whole device mass or volume. In the reported stack[12], the ECP-CNT composite was manually coated onto the titanium (Ti) bipolar plates by cast-evaporation, but a more industrially adaptable coating method should be used for further development. Herein, we report results from our recent effort to screen-print coatings of ECP-CNT composites onto Ti plates, and test them in supercapacitors of both single cells and bipolarly stacked multiple cells.

Screen-printing is a well-established technique for the preparation of electrodes, particularly in electrochemical sensors [14-15]. Due to its low cost, high reproducibility, and good ability to control thickness and area, screen-printing is also recommended for the fabrication of supercapacitor electrodes, as exemplified in the recent demonstration of a cobalt hydroxide (β-$Co(OH)_2$) thin film supercapacitor [16]. However, screen-printing is not yet well studied for fabrication of CNTs based electrode materials. This is possibly because CNTs often have high rigidity, large aspect ratio, and curvy shape[17]. As a result, CNTs based materials, such as their composites with ECPs, exhibit relatively low processability. Specifically for screen-printing, preparation of an effective ink of the ECP-CNT composite with a desired formulation and rheological property is of utmost importance[18]. Ideally, the ink should be both spreadable and viscous enough to remain on the screen before printing, although the rheological property is less important for printing on porous and hygroscopic (for aqueous inks) substrates, such as the separator (membrane)[18]. In this work, formulation of stable and printable inks of the ECP-CNT composites was achieved with the aid of suitable surfactant and binder. The surfactant is needed to improve the rheological property of the ink by reducing the surface tension of the aqueous solution on, and hence helps dispersion of the active materials. The binder can increase the mechanical strength of the screen-printed films. Nevertheless, surfactants and binders are non-conductive and non-capacitive, and hence likely impact electrode performance as will be discussed in this paper.

2 Experimental

2.1 Acid Treatment of Carbon Nanotubes

As-received multi-walled CNTs (diameter: 10 ~ 30 nm; length: 5 ~ 15 μm; Shenzhen Nanotech Port Co., Ltd) were treated in mixed HNO_3 (69%)

and H_2SO_4 (98 %) (V_{HNO_3}:$V_{H_2SO_4}$ = 1:3) under refluxation for 20 min to enable surface oxygenation, and removal of metallic residuals (catalysts) and amorphous carbon[8,12,19-20]. The produced black liquor was cooled to room temperature, washed in a filter crucible (grade 4.5) with deionised water (water in later text) until pH≈7, and oven-dried overnight (50 °C). The dry product could be re-dispersed in water readily after grinding with mortar and pestle.

2.2 Synthesis of Composites of ECP-CNTs

1) Composite of Polypyrrole and CNTs (PPy-CNT)

Acid treated CNTs (0.5 g) were dispersed in water (500 mL), followed by addition of pyrrole (2 g, Acros Organics, 99%) under sonication (20 min). Anhydrous $FeCl_3$ (10 g, Sigma-Aldrich, 97%) was dissolved in water (50 mL). The $FeCl_3$ solution was added under stirring into the pyrrole-CNT suspension drop by drop (interval = 1 s). The mixture was then filtered via a crucible filter (porosity 4). The black filtrand was washed until the water became colorless, dried at 40 °C for 24 h, weighed and ground to a fine powder. For comparison, another PPy-CNT composite was synthesised in 100 mL water with other experimental conditions remaining the same. For convenience, the two PPy-CNT composites prepared in 500 mL and 100 mL water are denoted as PPy-CNT_{500} and PPy-CNT_{100}, respectively, in this paper. In other cases, the mentioned PPy-CNT composite refers to PPy-CNT_{500}.

2) Composite of Polyaniline and CNTs (PAn-CNT)

Aniline (2 g, Sigma-Aldrich, > 99.5%) and then the acid treated CNTs (0.5 g) were added to 1 mol·L^{-1} HCl (100 mL), followed by sonication (20 min). A solution of $FeCl_3$ (10 g) in 1 mol·L^{-1} HCl (20 mL) was added to the aniline-CNT suspension drop by drop (interval = 1 s). The remaining procedures were the same as for preparation of PPy-CNT.

2.3 Electrode Fabrications

1) Cast-Evaporation

The powdery active material and polyvinyl alcohol (PVA, Sigma-Aldrich, > 98.1%) as a binder were thoroughly mixed at a mass ratio of 95:5 in an appropriate amount of water to form a stable dispersion. An electronic micropipette (EDP3 Rainin LTS 10 ~100 μL with wide orifice tips) was used to cast the dispersion onto a graphite disc electrode (diameter: 6.0 mm) which was made by covering the side wall of the graphite rod with epoxy resin, leaving the two ends open. After drying in air, the cast dispersion turned into a thin coating on the graphite disc (mass loading density: 0.3 ~ 3.0 mg·cm^{-2}).

2) Ink Preparation for Screen-Printing

It was found in this work that to screen print a relatively thick coating (e.g. 0.5 mm in thickness, or 50 mg·cm^{-2} in mass loading), the ink must be sufficiently thick (or viscous) to avoid flow after it was printed on the substrate. Such printable inks were prepared by mixing the active material, e.g. PPy-CNT, PAn-CNT or a specialty activated carbon (Cabot Monarch 1300 pigment black, CMPB) [12], with benzethonium chloride (BTC, Sigma-Aldrich, >98%) as surfactant, PVA as binder, and water as solvent in designated mass proportions. It was found that to obtain similarly stable and printable inks, the binder could be added at a much smaller amount for PPy-CNT or PAn-CNT than for CMPB, or even completely avoided when printing thin coatings.

When freshly made, the printable ink appeared as exemplified in Fig. 1A, and could be turned into a uniform coating on either a metal plate or a separator membrane (filter paper in this work, Whatman®, grade 1) using a manual screen-printer. The coating thickness was controlled by the stencil design thickness and the mesh screen opening size. Fig. 1(B, C) display screen-printed CMPB and PPy-CNT coatings on Ti plates (thickness: 0.1 mm) via a mesh screen of 0.24 mm in opening size.

2.4 Unit Cell Supercapacitors with Screen-Printed Electrodes

With the configuration illustrated in Fig. 2(A ~ C), two unit cell asymmetrical supercapacitors were fabricated as described here. Note that the mass loading of the active material on each electrode was selected to make the positive and negative elec-

trodes equal in capacitance.

"PPy-CNT (+) | 3 mol·L^{-1} KCl | CMPB (−)": PPy-CNT (300 mg) was thoroughly mixed with BTC (16 wt%, solid mass), PVA (4 wt%) and water (3 mL) to produce an ink which was then printed as a stable and fairly uniform coating over an area of 2 × 2 cm^2 (mass loading density: 75 mg·cm^{-2}) on a Ti plate as the positive electrode. (Note: all mass loading density values reported in this paper are with reference to the active material only.) Then, CMPB (490 mg) with BTC (16 wt%) and PVA (4 wt%) were dispersed in water (3 mL) and printed over an area of 2 × 2 cm^2 (mass loading density = 122.5 mg·cm^{-2}) on another Ti plate as the negative

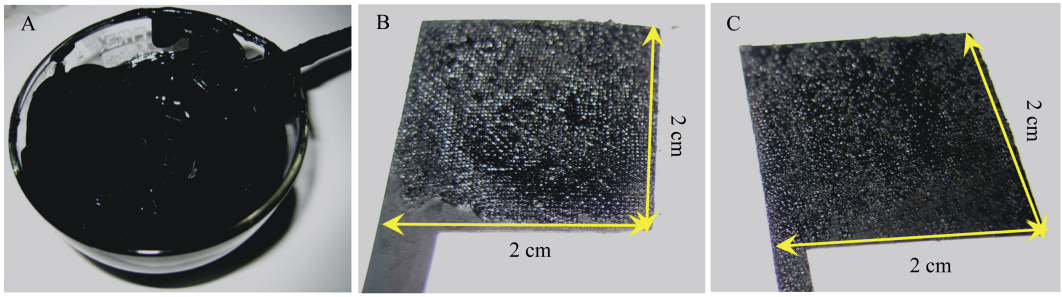

Fig. 1 Photographs of a typical ECP-CNT ink for screen printing (A), and screen printed CMPB (B) and PPy-CNT (C) composite on Ti plates.

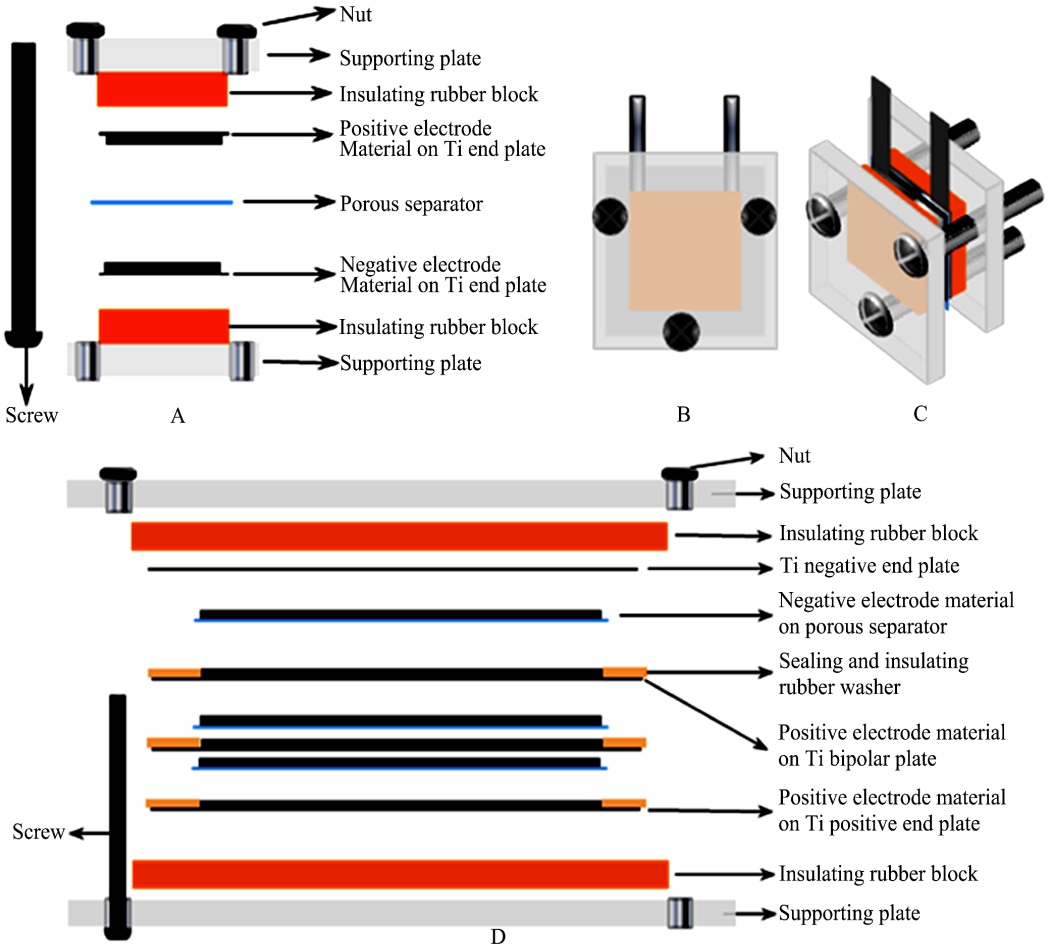

Fig. 2 Schematic illustrations of the expanded cross section (A), top (B), and three dimensional views (C) of the unit cell asymmetrical supercapacitor, and the expanded cross section of the stack of three bipolarly connected asymmetrical supercapacitor (D). Both designs include screen printed electrodes.

electrode. These two Ti plates were assembled into a sandwich type unit cell with a filter paper as the separator. The electrolyte was 3 mol·L^{-1} KCl, and was pre-added to the screen-printed coatings and the filter paper before assembly as illustrated in Fig. 2A. The amount of electrolyte applied was regarded as sufficient when further absorption of the liquid became impossible by the coatings and filter paper.

"PAn-CNT (+) | 1 mol·L^{-1} HCl | CMPB (−)": This cell was fabricated in almost the same way as described above for the PPy-CNT cell, except that the PAn-CNT ink was prepared without using the PVA binder. The positive electrode was PAn-CNT (53.9 mg, or 13.5 mg·cm^{-2}) with BTC (20 wt%), and the negative electrode was CMPB (100 mg, or 25 mg·cm^{-2}) with BTC (20 wt%) and PVA (5 wt%). The electrolyte was 1 mol·L^{-1} HCl and was applied in the same way for making the PPy-CNT cell.

2.5 Multi-Cell Stack of Supercapacitors with Screen-Printed Bipolar Electrodes

Addition of surfactant and binder helped preparation of inks, but also made the printed coatings more resistive. This effect was expected to be summative in the multi-cell stack. Also, the use of an acidic electrolyte for PAn-CNT caused concerns in the highly demanding manual fabrication of the multi-cell stack. Thus, as a first demonstration of screen-printing for making supercapacitor stacks, it was decided to make the PPy-CNT ink with a smaller amount of surfactant and no binder, although this meant a thinner coating. PPy-CNT with BTC (16 wt%) was printed on the positive side of the Ti plate (mass loading density: 14 mg·cm^{-2}). CMPB with BTC (16 wt%) and PVA (4 wt%) was printed on the separator (filter paper, mass loading density: 25 mg·cm^{-2}) on the side in contact with the negative side of the Ti plate. The printed area was 10 × 10 cm^2. Such printed Ti mono- and bipolar plates and separators were assembled into a three-cell stack according to Fig. 2D.

2.6 Equipments

The PGSTAT30 Autolab Potentiostat was used for all electrochemical control and measurements, including cyclic voltammetry (CV), galvanostatic charging and discharging (GCD) and electrochemical impedance spectroscopy (EIS), with or without using a reference electrode of Ag/AgCl (3 mol·L^{-1} KCl). Elemental analyses were carried out on the Thermo Scientific FlashEA 1112 organic elemental analyzer. The chemically synthesised ECP-CNT composites were inspected on the FEI-QUANTA 600 scanning electron microscope (SEM) and JEOL JEM-2100F high resolution transmission electron microscope (HRTEM). The screen-printed coatings were prepared on a Manual Mascoprint Compact Unit Screen Printer and inspected on an Intel ® QX3™ Computer Microscope.

3 Results and Discussion

3.1 Appearance of Printable Inks and Screen-Printed Coatings

For the three active materials (PPy-CNT, PAn-CNT and CMPB) studied in this work, attempts were made to formulate them into printable inks with the aid of surfactants with or without a binder. Three surfactants, benzethonium chloride (BTC), Triton X-100, and a domestic washing liquid, and three binders, polyvinyl alcohol (PVA), polytetrafluoroethylene and polyvinylidene fluoride were tested in this work with a total addition of 16 to 37 wt% of the active material. While making printable inks succeeded in most tested formulations with the appearance as exemplified in Fig. 1A, the printed coatings performed very differently in electrochemical tests. Considering conductivity and capacitance, it was finally decided to use BTC (ionic and hydrophilic) and PVA (hydrophilic) to carry out further tests with the total addition being not higher than 20 wt%.

The screen-printed coatings presented the mesh pattern on their surfaces, as shown in Fig. 1 (B, C) and Fig. 3(A ~ C). Such patterns were obviously because the ink was made sufficiently thick to avoid deformation via gravity driven flow after being printed on the substrate. However, these patterns al-

so made the coating surface uneven, which may increase the ionic contact area of the coating with a liquid electrolyte, and hence reduce the resistance of the cells and improve materials utilisation. However, when in contact with the separator membrane in a supercapacitor containing an insufficient amount of liquid electrolyte, the uneven surface of the printed coating could cause poor contact and hence underperformance. In addition to ensuring enough electrolyte in the cell, maintaining an appropriate pressure may also be necessary to improve the coating-membrane contact. This is because both the coating and separator membrane are soft and porous materials, and can deform under pressure to adapt each other's surface shapes. The pressure effect was often observed in this laboratory[12]. Note that the screen-printed coating of PAn-CNT in Fig. 3C is not as uniform as the other two in Fig. 3(A, B). It could have resulted from PAn forming more agglomerates, instead of coating on the CNTs as explained below.

3.2 Microscopy of Chemically Synthesised Composites of ECPs and CNTs

Fig. 4 compares previously reported SEM images of two chemically synthesised PPy-CNT composites[12] with that of a similarly synthesised PAn-CNT composite of this work. Both PPy-CNT and PAn-CNT showed curvy nanofibrils interconnected into a coralloid network. Chemically synthesised pure PPy exhibits typically microscopic features of lumps of various sizes[8]. Thus, the absence of such lumps in Fig. 4 (A, B) suggests the polymer to be well distributed on individual CNTs, which should help homogenize the properties of the composites, such as conductivity and electrochemical activity. The diameters of the PPy-CNT fibrils in Fig. 4 (A, B) were found to be 130 nm and 374 nm, respectively. However, the PAn-CNT composite contained fibrils of smaller diameters (ca. 75 nm on average), and also some agglomerates as shown in Fig. 4C. It could be because, in the acidic solution for PAn-CNT synthesis, the CNTs lost partially their negative charges due to protonation, and hence became less attractive to the positively charged polymer chains. As a result, some polymer chains aggregated to associate with small anions in the solution, particularly the Cl^- ions from $FeCl_3$ and HCl used in the synthesis.

The PPy-CNT and PAn-CNT nanofibrils were also studied by HRTEM. Typical results are presented in Fig. 5, showing clearly amorphous coatings on

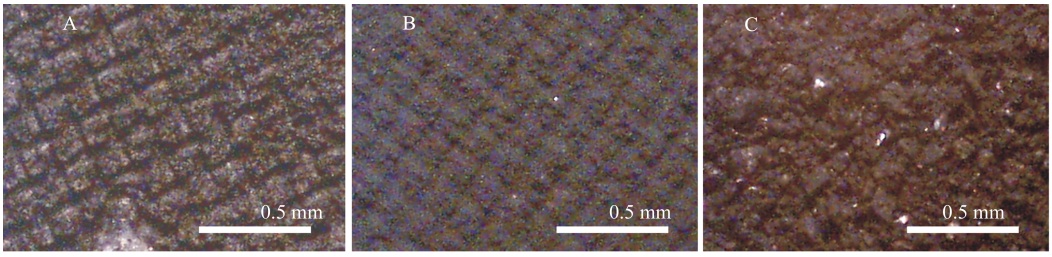

Fig. 3 Optical microscopic images of screen-printed coatings of CMPB (A), PPy-CNT composite (B), and PAn-CNT composite on Ti plates (C).

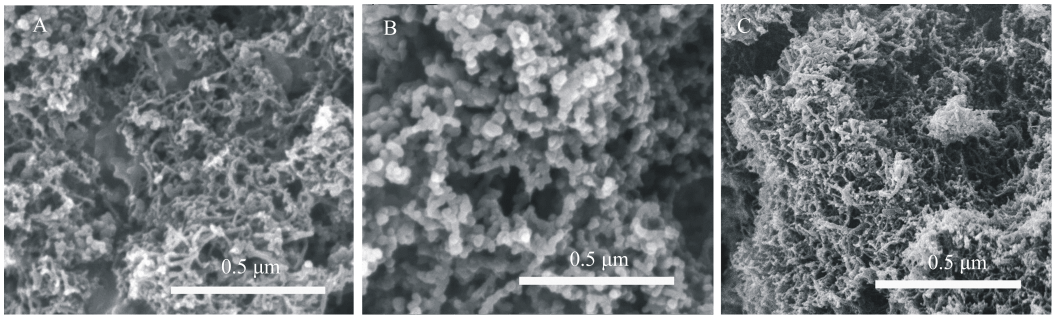

Fig. 4 SEM images of the PPy-CNT composites (A, B) synthesised in 500 mL ($PPy\text{-}CNT_{500}$) (A) and 100 mL ($PPy\text{-}CNT_{100}$) (B) water[12], and the PAn-CNT composite synthesised in 100 mL water (C).

each CNT. It has been confirmed that the amorphous carbon in the as-received CNTs can be removed by acid treatment[8,20]. Thus, the coatings on the CNTs in Fig. 5 should be PPy or PAn. Furthermore, the PPy-CNT_{500} fibril in Fig. 5A shows a thinner coating (ca. 5.0 nm) than that (ca. 8.5 nm) of PPy-CNT_{100} in Fig. 5B. It should be mentioned that well resolved HRTEM images were only obtained on CNTs with relatively thin coatings. Thus, Fig. 5 is reported here as evidence of uniform polymer coatings on individual CNTs, instead of representing the coating thickness in the PPy-CNT or PAn-CNT samples examined.

It is worth noting that the uniform coatings of PPy or PAn on individual CNTs as presented in Fig. 5 suggest that the polymer could wrap each CNT. This is strong evidence that the polymers were attached to the CNTs through not only the negatively charged surface groups of CNTs (resulting from partial oxidation in the acid treatment)[19], but also the π-π stacking because chemical bonds in both conducting polymers and CNTs are highly conjugated[21].

3.3 Elemental Analysis

Elemental compositions (wt%) of the ECP-CNT composites and similarly prepared pure ECPs are listed in Tab. 1. The greater carbon contents in the composites than that in the respective pure ECPs agree with the presence of CNTs in the former. The PAn-CNT composite contained 74.27 wt% carbon, equivalent to 57.91 wt% CNTs, in contrast to the synthesis target of 25 wt% CNTs. Such a high CNT content means that the PAn coatings on individual CNTs should be fairly thin, which agrees with the SEM and HRTEM observations. Again, it is because PAn tended to form aggregates in association with the small anions in the solution, rather than grow on the CNTs which had lost partly their negative surface charge due to protonation in the acidic synthesis solution. Some of these PAn aggregates may be too small to be retained by the filter, and not be collected for analysis. The CNT content in PPy-CNT_{500} was 26.88 wt%, close to the synthesis aim of 25 wt%. PPy-CNT_{100} contained 9.99 wt% CNTs, further confirming that the PPy coating thickness could be fairly well controlled by the volume of the synthesis solution, in agreement with the SEM observations reported in Section 3.2.

3.4 Electrochemical Characterisations

The obtained ECP-CNT composites were first

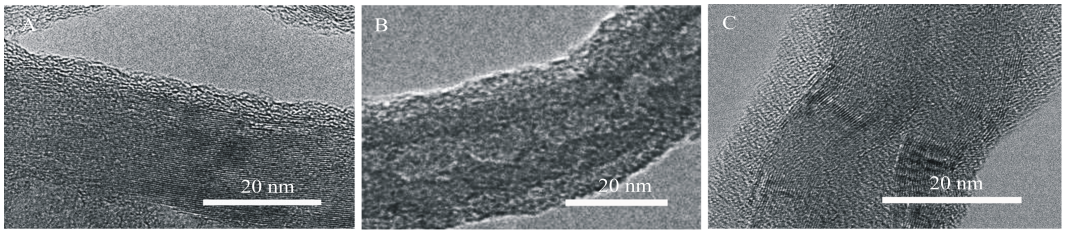

Fig. 5 HRTEM images of PPy-CNT nanofibrils (A, B) synthesised in 500 mL (PPy-CNT_{500}) (A) and 100 mL (PPy-CNT_{100}) (B) water, and PAn-CNT nanofibrils synthesised in 100 mL water (C).

Tab. 1 Elemental composition (wt%) of CNTs, ECPs and ECP-CNT nanocomposites

Samples\element	N	C	H	S	O
Acid treated CNTs	0.00	86.57	0.37	0.00	13.06
PPy	14.04	50.67	3.50	0.00	31.79
PAn	9.78	57.35	4.42	0.00	28.45
PPy-CNT^{a}_{500}	12.13	60.32	2.77	0.29	24.49
PPy-CNT^{b}_{100}	15.47	54.22	3.79	0.00	26.52
PAn-CNT^{c}	2.74	74.27	1.25	0.00	21.74

[a,b,c] Synthesised in 500(a), 100(b) and 100(c) mL water.

coated on the working electrode (graphite disc: 6 mm in diameter) by cast-evaporation and studied in a three-electrode cell with a naked graphite rod counter electrode (6 mm in diameter and about 2 cm in immersion depth), and a Ag/AgCl (3 mol·L^{-1} KCl) reference electrode. It is well known that PPy is active in neutral aqueous electrolytes, whilst PAn in acidic aqueous electrolytes [8,12-13,19,21-22]. Thus, in this work, the PPy-CNT and PAn-CNT samples were investigated in neutral and acidic aqueous electrolytes, respectively.

Fig. 6 shows the cyclic voltammograms (CVs) of PPy-CNT_{500} (A) and PPy-CNT_{100} (B) at different mass loadings on the working electrode in 0.5 mol·L^{-1} KCl aqueous solution. Both samples showed an increasing current (or capacitance) with increasing the mass loading. A comparison of the CVs revealed interesting differences between the two samples. Firstly, the CVs in Fig. 6B are not as rectangular as those in Fig. 6A, showing slow current switching at the negative potential end. Secondly, at more positive potentials, the CV currents in Fig. 6B are larger than those in Fig. 6A. These differences could be attributed to PPy-CNT_{100} containing more PPy (see Tab. 1) which would be more resistive at negative potentials, but contribute to the oxidation current at positive potentials.

As displayed in Fig. 7, the galvanostatic charging and discharging plots (GCDs) of the two PPy-CNT composites exhibited satisfactory linear potential-time relationships in the potential range from −0.5 to 0.5 V, suggesting the capacitive nature

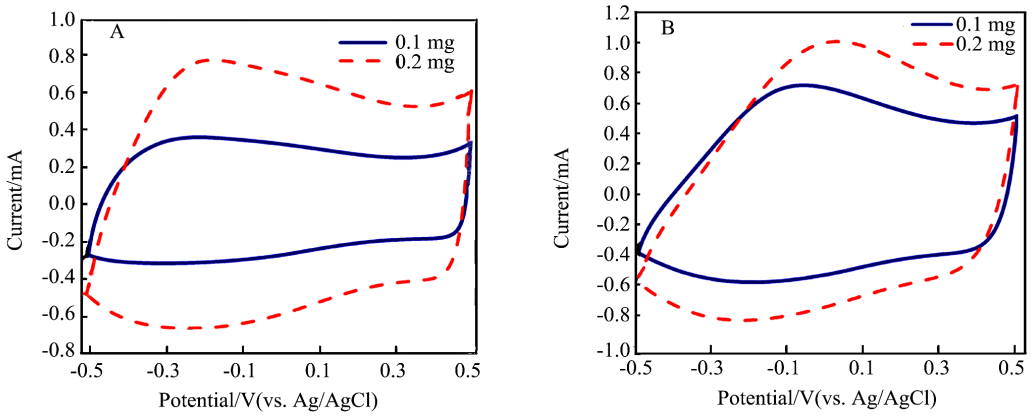

Fig. 6 CVs of PPy-CNT synthesised in 500 mL (PPy-CNT_{500}) (A) and 100 mL (PPy-CNT_{100}) (B) water in a three electrode cell. Working electrode: PPy-CNT on graphite disc of 6.0 mm in diameter at mass loadings as indicated. Counter electrode: Graphite rod of 6.0 mm in diameter. Electrolyte: 0.5 mol·L^{-1} KCl aqueous solution. Scan rate: 10 mV·s^{-1}.

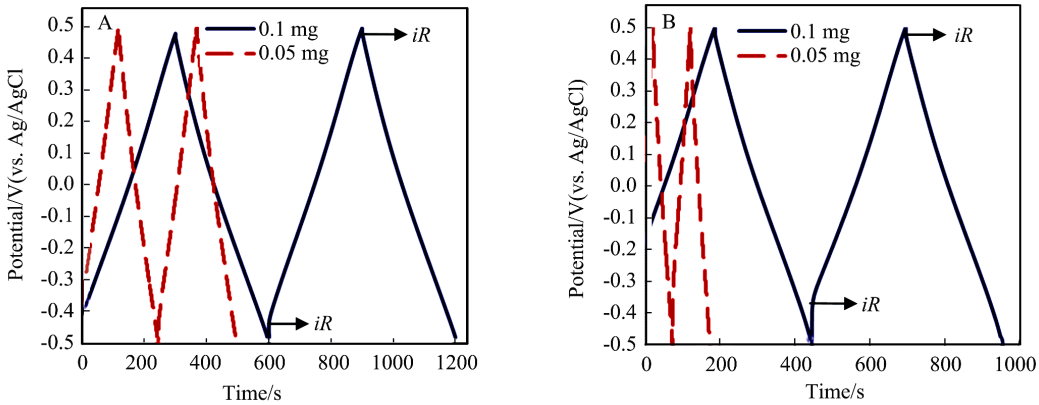

Fig. 7 GCD plots of PPy-CNT synthesised in 500 mL (PPy-CNT_{500}) (A) and 100 mL (PPy-CNT_{100}) (B) water in a three electrode cell. Working electrode: PPy-CNT on graphite disc of 6.0 mm in diameter at mass loadings as indicated. Counter electrode: Graphite rod of 6.0 mm in diameter. Electrolyte: 0.5 mol·L^{-1} KCl aqueous solution. Constant current: 0.2 mA.

of charge transfer reactions on the electrodes. However, the GCDs of PPy-CNT$_{100}$ presented larger *iR* drops (indicated by the vertical section upon switching the current) at the negative potential ends than those of PPy-CNT$_{500}$. Conversely, at the positive potential ends, there were very small signs of the *iR* drop on the GCDs of both samples. It can be explained by PPy being less conductive at negative potentials. Thus, the composite containing more PPy would be more resistive at negative potentials. These results are in good agreement with the observations on, and analyses of the CVs.

CVs of the PAn-CNT composite in 1 mol·L^{-1} HCl aqueous solution are presented in Fig. 8A. In the potential window ranging from 0.1 to 0.7 V (vs. Ag/AgCl), the CV of 0.4 mg mass loading is not as rectangular as that of a lower mass loading, suggesting a larger resistance of the thicker coating. Also, the CV current of PAn-CNT is not as smooth as that of PPy-CNT. It could have resulted from PAn having three oxidation states[8,21-22]. The absence of clear current peaks in Fig. 8A may be attributed to that the PAn in the composite was never fully reduced in the explored potential range[8], and that the CNTs helped delocalisation of charge transfer in the composite[21].

Fig. 8B shows the GCDs of PAn-CNT at two mass loadings in the potential range from 0.1 to 0.7 V, exhibiting satisfactory capacitive features. The GCDs also show quite small *iR* drops at both potential ends, likely because PAn in the coatings was never fully reduced in the testing potential range.

3.5 Unit Cell Asymmetrical Supercapacitors with Screen-Printed Electrodes

Supercapacitors have traditionally symmetrical configurations with the positive and negative electrodes being of the same material in equal mass, but are now progressing into asymmetrical types [12,23-24] with different positive and negative electrode materials to gain improved performance. In the asymmetrical case, the total cell capacitance is determined by Eq. 1.

$$\frac{1}{C_{cell}} = \frac{1}{C_+ \times m_+} + \frac{1}{C_- \times m_-} \quad (1)$$

where C_{cell} is the total cell capacitance, C_+ and C_- are specific capacitance values, and m_+ and m_- are masses of the positive and negative electrode active materials, respectively. The maximum specific power, P_{max}, of the cell can be calculated according to Eq. 2 below[24],

$$P_{max} = \frac{U^2}{4ESR}\left(\frac{1}{m}\right) \quad (2)$$

where U is the cell voltage, ESR the equivalent series resistance of the cell, and $m = m_+ + m_-$. Eq. 2 can be explained by Scheme 1 with P, I, R_L and R being the output power of the power source, current, resistance of the load, and the total resistance of the circuit, respectively. The specific energy, E_s, of the cell can be derived using the following equation,

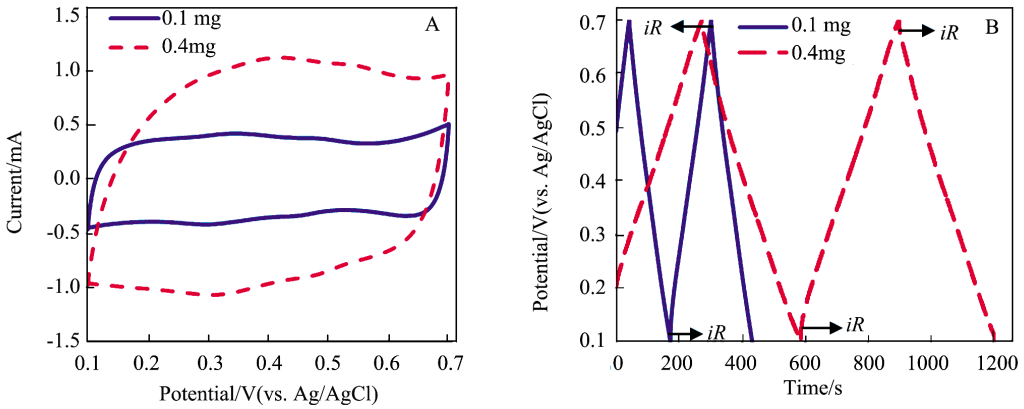

Fig. 8 Electrochemical characterisations of the PAn-CNT composite of different mass loadings as indicated in a three electrode cell containing 1 mol·L^{-1} HCl aqueous solution. CVs at a scan rate of 10 mV·s^{-1} (A). GCDs at constant currents of 0.2 mA (B). A 6.0 mm diameter graphite rod was used as the current collector.

$$E_s = \frac{C_{cell}U^2}{2m} \quad (3)$$

In previous sections, electrochemical characterisations were achieved on coatings of PPy-CNT and PPy-PAn prepared by cast-evaporation. The same method was previously applied to make PPy-CNT (+) and CMPB (−) electrodes for fabrication of a prototype asymmetrical supercapacitor that performed well in the capacitive manner[12]. Although a common and convenient practice of manual work in laboratory, cast-evaporation is rarely used at industrial scales, mainly because it is slow in evaporation, and inaccurate in controlling the dimensions and mass content of the coating.

An alternative and commercially established method is screen-printing which can offer better controls on dimensions, particularly thickness, of the coatings. Formulation and preparation of printable inks were a main task in this work as described in Sections 2.3 to 2.5, 3.1, and Fig. 1 and 3. It should be mentioned that the screen-printed coatings in this work were not studied individually in the three-electrode cell. This is because the manual printer used in this work could only produce coatings with relatively large areas. Therefore, the following discussion is focused on the performance of the screen-printed coatings in two-electrode cells, e.g. unit cell supercapacitors and also bipolarly connected multi-cell stacks as illustrated in Fig. 2[12,24].

The two unit cell asymmetrical aqueous supercapacitors studied in this work were "PPy-CNT (+) | 3 mol·L^{-1} KCl | CMPB (−)" and "PAn-CNT (+) | 1 mol·L^{-1} HCl | CMPB (−)" as described in Section 2.4. Results from electrochemical characterisations of these two cells are presented in Fig. 9. At all applied scan rates, the CVs (A and C) of both cells were fairly rectangular in shape between 0.0 to 1.0 V. However, an increasing current at voltages near 1.0 V can be seen in Fig. 9A, but not in Fig. 9C. A possible explanation may come from a comparison between Fig. 6 and 8, which also show an increasing current near the positive limit of the potential scan. However, the potential for this increasing current was 0.5 V for PPy-CNT, but 0.7 V for PAn-CNT. Thus, if the CMPB negative electrode in the two supercapacitors experienced the same potential change when the cell voltage was increased from 0 to 1.0 V, the positive electrode could have reached a potential near or beyond 0.5 V but below 0.7 V. Consequently, the PPy-CNT electrode would experience the same change as that shown in Fig. 6, giving rise to the increasing current at voltages near 1.0 V in Fig. 9A.

As mentioned in Section 2.5, the use of binder and/or surfactant in the electrode materials would increase the resistance of the cell. To study such effects, GCDs of the two supercapacitors were purposely recorded at currents much higher than those observed on the CVs. As shown in Fig. 9B and D, significant *iR* drops were observed. It is worth mentioning that the overall cell voltage, U, is the sum of the potential difference between the positive and negative electrodes, ΔE, and the iR drop, i.e. $U = \Delta E + iR$, where ΔE is needed to charge or discharge the cell. Thus, a large *iR* drop means a smaller ΔE. As a result, little or no non-capacitive change occurred in the cell, leading to almost ideal capacitive responses as represented by the straight slope

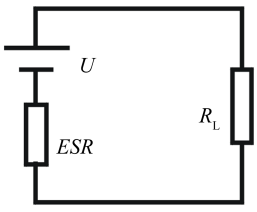

$$P = IU = I^2 R_L$$

$$I = \frac{U}{R} \qquad R = R_L + ESR$$

$$P = R_L \left(\frac{U}{R_L + ESR} \right)^2 = \frac{R_L U^2}{(R_L + ESR)^2}$$

$$At\ R_L = ESR \Rightarrow P = P_{max} = \frac{U^2}{4ESR}$$

Scheme 1 Equivalent circuit of a supercapacitor (voltage = U) with its equivalent series resistance (ESR) and external load (R_L) (Left). Derivation of the maximum output power of the supercapacitor (Right).

portions on the GCDs in Fig. 9. Nevertheless, it can still been seen in Fig. 9B that the charging branch of the GCD is slightly curved at potentials near 1.0 V, which is indicative of the same non-capacitive contribution as observed on the CV in Fig. 9A.

From the *iR* drops observed on the GCDs, the *ESR* values were calculated to be 1.8 Ω for "PPy-CNT (+) | 3 mol·L^{-1} KCl | CMPB (−)" and 2.1 Ω for "PAn-CNT (+) | 1 mol·L^{-1} HCl | CMPB (−)". These *ESR* values are not negligible and can be partly attributed to the effect of the non-conductive surfactant and binder. However, it is surprising that the resistance of the PAn-CNT cell was slightly larger than that of the PPy-CNT cell. Because the PAn-CNT coating contained no binder (PVA), but more CNTs, and was less loaded than the PPy-CNT coating, the slightly larger *ESR* of the PAn-CNT cell should have not resulted from the PAn-CNT coating itself, but was more likely due to a poorer contact between the coating and the separator membrane as mentioned in Section 3.1 and Fig. 3C.

It can be derived from the CV and GCD results that the value of C_{cell} ranged between 1.77 and 2.12 F for the PAn-CNT cell, and 2.96 and 3.39 F for the PPy-CNT cell, depending on the rate of charge-discharging. The higher capacitance of the latter can be attributed to the higher mass loading density (75 mg·cm^{-1} for PPy-CNT vs. 14 mg·cm^{-2} for PAn-CNT). However, upon normalisation, the thicker PPy-CNT coating does not represent an advantage as shown in Tab. 2 together with other normalised properties. It is worth mentioning that a previously reported supercapacitor stack fabricated from PPy-CNT approached 25 kW·kg^{-1} in maximum specific power[12], which is much larger than that of both the PAn-CNT and PPy-CNT cells as listed in Tab. 2.

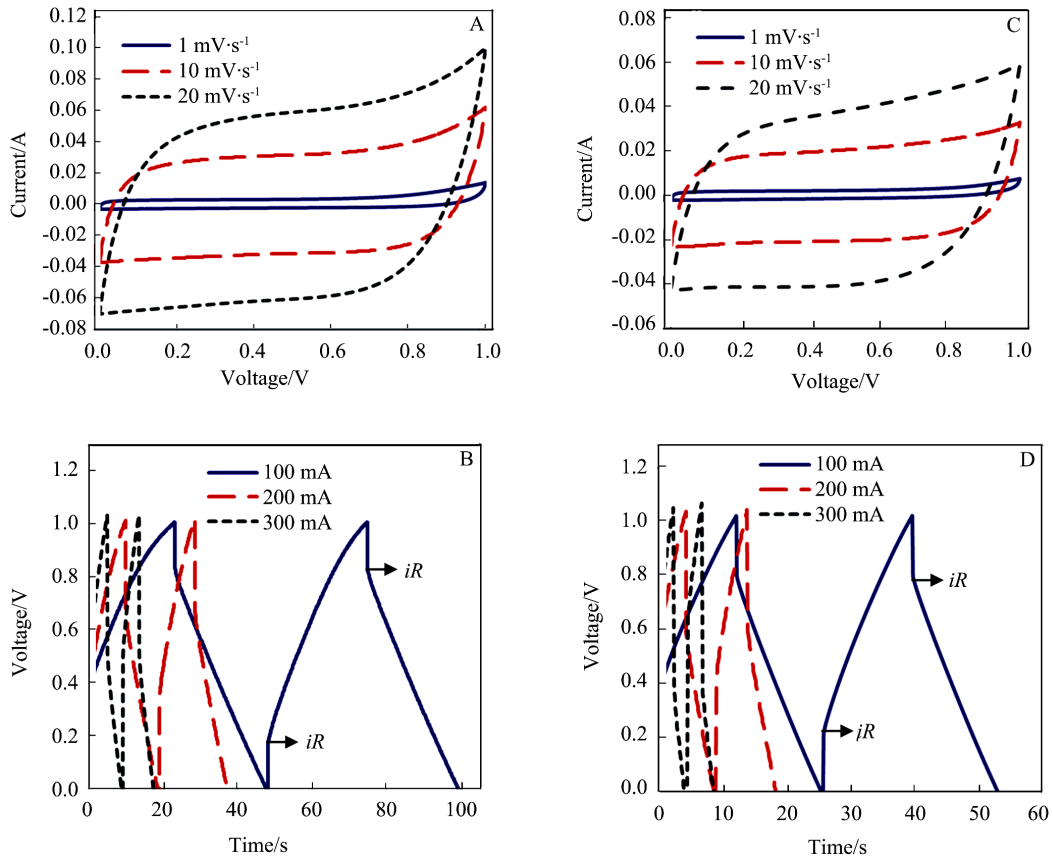

Fig. 9 CVs at indicated scan rates (A, C), and GCDs at indicated constant currents (B, D) of unit cell asymmetrical aqueous supercapacitors of "PPy-CNT (+) | 3 mol·L^{-1} KCl | CMPB (−)" (A, B), and "PAn-CNT (+) | 1 mol·L^{-1} HCl | CMPB (−)" (C, D). The current collectors were titanium plates with a screen-printed area of 2 × 2 cm^2.

The cause could be attributed to the thicker coatings, but also likely to the use of the non-conductive surfactant and binder which could impact negatively the utilisation of the active material on the electrode.

3.6 Stack of Three Asymmetrical Supercapacitors with Screen-Printed Bipolar Electrodes

Electrochemical energy conversion and storage devices, including supercapacitors, usually have a single cell voltage ranging from 1.0 V (aqueous electrolyte) to 3.5 V (organic electrolyte). Charging the device to higher voltages will lead to either over-oxidation, or over-reduction, or decomposition of a component of the cell, particularly the active electrode materials and the solvent. To achieve high device voltages for designated applications, serially stacking the cells through bipolar electrodes is a preferred approach[12,24-27].

In this work, a three-cell stack was fabricated from the printed PPy-CNT coating on the Ti bipolar plate (10×10 cm^2) and the CMPB coating on the filter paper as described in Section 2.5 and illustrated in Fig. 2D. In Fig. 10A, typical CVs of the stack are presented over a voltage window of 3.0 V, considering that each cell was tested to 1.0 V as shown in Fig. 9(A, B). The CV of the stack was very similar to that of the single cell, featuring a fairly rectangular shape with an increasing current at voltages near the high voltage end. This increasing current is more pronounced on the CV of the stack, suggesting a summative effect from the three cells in the stack.

Note that the voltage scan rate of 5 mV·s^{-1} for the stack corresponds to an average scan rate of 5/3 = 1.67 mV·s^{-1} for each of the three cells in the stack. The capacitive current is proportional to the voltage scan rate, v, and the total mass of active materials, m, on both the positive and negative electrodes. Thus, it is possible to compare the performances of the screen-printed electrodes in the single cell and in the three-cell stack by using the normalised current, $I_m = \frac{i}{vm}$. It can then be derived that I_m = 3.8 A·s·V^{-1}·g^{-1} (= F·g^{-1}) (at 10 mV·s^{-1}) from Fig. 9A, and I_m = 19.2 A·s·V^{-1}·g^{-1} (at 5 mV·s^{-1}) from Fig. 10A. Such a large difference in I_m might have resulted largely from the very different electrode mass loading densities between the single cell and the stack. On the PPy-CNT(+) electrode, the mass loading density was 75 mg·cm^{-2} in the single cell, but only 14 mg·cm^{-2} in the stack. On the other hand, if the current is normalised against the electrode area, S, i.e., $I_S = \frac{i}{vS}$, it can then be derived that I_S = 0.75 A·s·V^{-1}·cm^{-2} (= F·cm^{-2}) from both Fig. 9A and 10A. In other words, the thicker coating did not show an added advantage. These analyses suggest much poorer utilisation of the active material in the thicker screen-printed coatings. The effect could also be partly attributed to the non-conducting surfac-

Tab. 2 Normalised capacitance, energy, and maximum power of unit cells of "ECP-CNT (+) | 3.0 mol·L^{-1} KCl | CMPB (-)"

Properties	PAn-CNT (CV)	PPy-CNT (CV)	PAn-CNT (GCD)	PPy-CNT (GCD)
C_{cell}/F	1.77	2.96	2.12	3.39
C_E/(F·cm^{-2})	0.89	1.48	1.06	1.70
C_M/(F·g^{-1})	65.6	19.7	78.5	22.6
E_s/(Wh·kg^{-1})	1.60	0.52	1.90	0.60
P_{max}/(kW·kg^{-1})	*N/A*		0.35	1.55

C_E: Electrode capacitance normalised against the printed electrode area.

C_M: Specific capacitance of ECP-CNT in the cell.

E_s and P_{max}: Specific energy and maximum specific power at 1.0 V with *ESR* from GCD, normalised against total mass of active materials on both +/- electrodes.

tant and binder impacting negatively on material utilisation.

The cyclic charge-discharge stability of the stack was checked by CVs as shown in Fig. 10A. Gradual decrease of the CV current was recorded with the stack capacitance dropping by about 25% after 500 charge-discharge cycles. The decay was noticeably faster than that reported for a 19 cell stack fabricated with similar PPy-CNT which was however coated on Ti substrates by case-evaporation with PVA as a hydrophilic binder to assist wetting of the active materials by the electrolyte but without using any surfactant[12]. Because PVC was used in both cases at similar concentrations, the capacitance decay observed in Fig. 10A may be largely attributed to the effect of the chain molecule of the surfactant, BTC, which could have been stretched in the freshly printed coating, but then relaxed gradually during the charge-discharge cycles. The exact cause for this negative effect of the surfactant requires further research to better understand and identify a solution.

The stack was also tested by GCD as shown in Fig. 10B. The constant current applied was 100 mA which is comparable with the currents on the CV in Fig. 10A. It can be seen that the GCDs are capacitive in nature, although the charging branches show non-capacitive distortion at voltages near 3.0 V. There are also minor differences between the two charge-discharge cycles in Fig. 10B. The second cycle took less time to complete, mainly because the charging branch of the second cycle exhibited a smaller non-capacitive distortion near 3.0 V. This non-capacitive feature on the GCDs may be attributed to the same causes as that on the CV. There are also vertical portions or *iR* drops on the GCDs in Fig. 10B, but the changes were too small to be reliably measured.

Alternatively, the stack was tested by EIS which can offer not only the resistance of the cell, but also other useful information. Fig. 10C shows the Nyquist plot of the three-cell stack measured at a cell voltage of 0 V to avoid complications from electrode reactions. The high frequency intercept of the impedance plot at the real impedance axis is 0.185 Ω which is effectively the *ESR* of the stack. Such a small *ESR* value explains the very small *iR* drop observed on the GCDs in Fig. 10B. This finding should not been seen as a decrease in the intrinsic resistivity of the printed PPy-CNT coating, but likely the combined influence of the smaller mass loading (14 $mg \cdot cm^{-2}$) and the larger printed area (100 cm^2) of the stack. According to Eq. 2, the maximum power of the stack can be calculated to be 12.2 W (or 1.04 $kW \cdot kg^{-1}$). The low frequency imaginary impedance is plotted against the reciprocal of the frequency in Fig. 10D, showing a straight line which not only confirms the capacitive origin of the data, but also helps derive from the slope a capacitance value of 21.5 F. This value is smaller than those measured from the CV (26.6 F) and GCD (30.3 F), which can be explained by the CV and GCD measurements having included non-capacitive contributions as discussed above. These stack capacitance values can be translated to other normalised properties as shown in Tab. 3.

In addition to the above analyses, the impedance plot also presents a semi-circle at high frequencies and a short inclined section between the semicircle and the capacitive line as shown in Fig. 10E. The short inclined section is not the same as the Warburg impedance which should be a straight line at an angle of 45° vs. the Z' axis, suggesting that charge transfer in the supercapacitor was not influenced significantly by diffusion. This feature is indicative of the printed coatings of the active materials being relatively thin and/or porous.

The high frequency semicircle is characteristic of a kinetic barrier to charge transfer through an interface between two contacting phases. In the supercapacitors, there could be three interfaces, i.e. the "Ti | composite" and "carbon | polymer" interfaces for electron transfer, and the "polymer | electrolyte" interface for ion transfer. It is known that the fre-

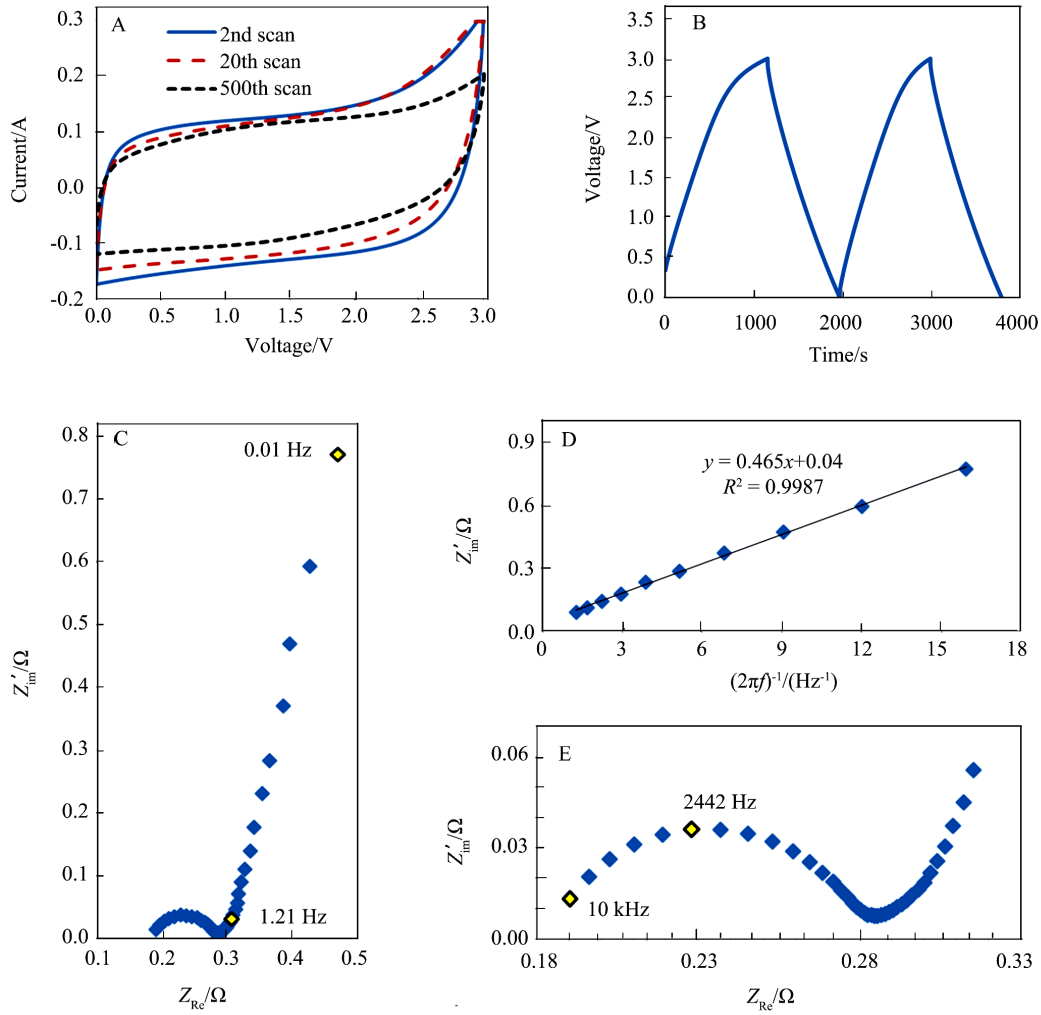

Fig. 10 Electrochemical characterisations of the stack of three asymmetrical supercapacitors, "PPy-CNT (+) | 3 mol·L^{-1} KCl | CMPB (−)", connected by screen-printed Ti bipolar plates of 10 × 10 cm^2 in printed area. A. CVs of the indicated potential cycles at 5 mV·s^{-1}; B. GCD plots at 100 mA; C. Nyquist plot recorded at 0 V between 0.01 and 10 kHz; D. A plot of imaginary impedance against reciprocal of frequency at low frequencies with the linear fitting result; E. Enlarged high frequency section of the Nyquist plot in (C).

quency of the maximum imaginary impedance on the semicircle, f_{max}, is related to the charge transfer resistance, R_{ct}, and the capacitance of the interface, C_{dl}, i.e. $2\pi f_{max} = \frac{1}{R_{ct}C_{dl}}$. From the two extrapolated intercepts of the semicircle with the Z' axis, R_{ct} was found to be about 0.10 Ω. It can then be calculated that C_{dl} = 0.65 mF. Of the three interfaces mentioned above, the "Ti | composite" interface had an area defined by the printed area on the Ti plate (100 cm^2). Normalising against this interface produced a value 39 μF·cm^{-2}. For the other two interfaces, the area would be much larger considering the small diameters of the CNTs and also the porous structures of the printed coatings. Considering that the true electrode capacitance is usually smaller than 40 μF·cm^{-2}[28], the semicircle shown in Fig. 10C or 10E may be reasonably attributed to the kinetic barrier to electron transfer crossing the "Ti | composite" interface.

4 Discussion on Specific Capacitance Values from Different Measurements

Unlike many studies reported in the literature, this work has tested three types of electrodes of considerably different surface areas, ranging from the

graphite disk of 0.28 cm^2 in cast area (0.6 cm in diameter) to the Ti plate with a printed area of 100 cm^2. The mass loading density also changed from 0.18 mg·cm^{-2} to 75 mg·cm^{-2} using two different methods, i.e. cast-evaporation and screen-printing. Whilst all these electrodes of different scales behaved in similar capacitive manners, the expected or desired proportionality was not observed. In particular, the measured specific capacitance was found to depend strongly on the mass loading density of the electrode.

For example, as derived from GCDs, the specific capacitance of PPy-CNT_{500} at a mass loading density of 0.35 mg·cm^{-2} was 589 F·g^{-1} (Fig. 7A). However, for the same material, the value dropped to 131 F·g^{-1} at 14 mg·cm^{-2} (Tab. 3), and 22.6 F·g^{-1} at 75 mg·cm^{-2} (Tab. 2). Such large discrepancies deserve a discussion. The very low value of 22.6 F·g^{-1} is understandable due to the thicker coating being unfavourable for ion penetration and hence utilisation of the active material. The presence of the non-conducting surfactant in the coating could also have impacted negatively. However, the very high value of 589 F·g^{-1} is suspicious. The theoretical specific capacitance of PPy is 619 ~ 495 F·g^{-1} as calculated from the monomer formula mass (67), charge transfer per monomer (1/3), and potential window (0.8 ~ 1.0 V), disregarding the dopant anion[28]. The specific capacitance of acid treated CNTs was reported to be about 50 F·g^{-1} [8]. The PPy content in PPy-CNT_{500} was 73.12 wt% (cf. Section 3.3 and Tab. 1), suggesting a contribution of 453 ~ 362 F·g^{-1}. Similarly, the contribution from CNTs would be less than 14 F·g^{-1}. Thus, the specific capacitance of PPy-CNT should not be higher than 467 F·g^{-1}.

It is possible to speculate several causes for the measured specific capacitance of 589 F·g^{-1}, whilst the following three are possibly more relevant. Firstly, PPy-CNT_{500} was highly porous at both micrometre and nanometre scales as shown in Fig. 4A, which could have contributed additional double layer capacitance. Secondly, to a minor degree, the graphite disc electrode should have its own capacitance which is proportional to the geometric surface area, surface roughness, and the actual double layer capacitance. This substrate contribution becomes more significant when the mass loading density decreases. Finally, the cast-evaporation method used to prepare the coating could have introduced a high inaccuracy in mass loading which was derived from the volume of the aqueous suspension of the PPy-CNT composite cast on the electrode surface. Obviously, unlike a true solution, the solid content in a very small volume of the PPy-CNT suspension as taken by the electronic micropipette (10 ~ 100 μL) could differ non-negligibly from that in the bulk suspension. A worse scenario could have resulted from the length and the high aspect ratio of the polymer coated CNTs.

Tab. 3 Normalised capacitance, energy, and maximum power of the three-cell stack of "PPy-CNT (+) | 3.0 mol·L^{-1} KCl | CMPB (-)" derived from different measurements

Properties	CV	GCD	EIS
C_{stack}/F	26.6	30.3	21.5
C_E/(F·cm^{-2})	1.60	1.83	1.29
C_M/(F·g^{-1})	114	131	92.1
E_s/(Wh·kg^{-1})	2.84	3.24	2.30
P_{max}/(kW·kg^{-1})	*N/A*		1.04

C_E: Electrode capacitance normalised against electrode area.

C_M: Specific capacitance of PPy-CNT in the stack.

E_s and P_{max}: Specific energy and maximum specific power at 3.0 V with *ESR* from EIS, normalised against total mass of active materials on all +/- electrodes in the stack.

5 Conclusions

This article has reported the preparation and application of screen-printed coatings of ECP-CNT composites, starting from chemical synthesis. The morphology and electrochemical properties of the chemically synthesised PPy-CNT and PAn-CNT composites were examined by visual inspection, SEM, HRTEM, CV, and GCD. It was found that if the synthesis was carried out in a solution with lower concentrations of monomer and CNTs, the product would have, on average, a thinner polymer coating on individual CNTs, but offer greater conductivity and higher capacitance. For PAn-CNT, a noticeable amount of the polymer was found to aggregate, instead of forming coatings on the CNTs. Between PPy-CNT and PAn-CNT, the former offered a wider potential window (-0.5 to 0.5 V vs. Ag/AgCl) in the neutral electrolyte of 3 mol·L^{-1} KCl than that of the latter (0.1 to 0.7 V) in 1 mol·L^{-1} HCl. For screen-printing, both PPy-CNT and PAn-CNT could be formulated into printable inks, although the former led to a smoother coating. When tested in unit cell asymmetrical supercapacitors with an activated carbon negative electrode of equal capacitance, the PAn-CNT cell behaved in a highly capacitive manner, whilst non-capacitive charging current was recorded in the PPy-CNT cell which nonetheless gave a lower *ESR* value. In particular, the screen-printed PPy-CNT coating on a printed area of 10 × 10 cm^2 was further tested in a three-cell stack with two Ti bipolar plates by CV, GCD and EIS. The results confirmed expected summative contributions from individual cells, including both capacitive and non-capacitive factors. Although far from optimisation, the three-cell stack showed several promising specifications, including 1.25 ~ 1.83 F·cm^{-2} in electrode capacitance, 2.3 ~ 3.2 Wh·kg^{-1} in specific energy, and 1.04 kW·kg^{-1} in maximum specific power. However, the cyclic charge-discharge stability of the stack was compromised possibly due to a relaxation effect of the surfactant used. Thus, this preliminary study calls for further research to develop screen-printing as a scalable technique for fabrication of ECP-CNT composites based electrodes in commercial supercapacitors.

Acknowledgement

The authors thank E.ON AG for funding through the E.ON International Research Initiative-Energy Storage 2007. Responsibility for the content of this paper lies with the authors.

References:

[1] Arabale G, Wagh D, Kulkarni M, et al. Enhanced supercapacitance of multiwalled carbon nanotubes functionalized with ruthenium oxide[J]. Chemical Physics Letters, 2003, 376(1/2): 207-213.

[2] Simon P, Gogotsi Y. Materials for electrochemical capacitors[J]. Nature Materials, 2008, 7(11): 845-854.

[3] Eliad L, Pollak E, Levy N, et al. Assessing optimal pore-to-ion size relations in the design of porous poly (vinylidene chloride) carbons for EDL capacitors[J]. Applied Physics A: Materials Science & Processing, 2006, 82(4): 607-613.

[4] Eliad L, Salitra G, Soffer A, et al. On the mechanism of selective electroadsorption of protons in the pores of carbon molecular sieves[J]. Langmuir, 2005, 21(7): 3198-3202.

[5] Frackowiak E, Béguin F. Carbon materials for the electrochemical storage of energy in capacitors[J]. Carbon, 2001, 39(6): 937-950.

[6] Vix-Guterl C, Frackowiak E, Jurewicz K, et al.Electrochemical energy storage in ordered porous carbon materials[J]. Carbon, 2005, 43(6): p. 1293-1302.

[7] Brownson D A C, Banks C E. Fabricating graphene supercapacitors: Highlighting the impact of surfactants and moieties[J]. Chemical Communications, 2012, 48 (10): 1425-1427.

[8] Peng C, Jin J, Chen G Z. A comparative study on electrochemical co-deposition and capacitance of composite films of conducting polymers and carbon nanotubes[J]. Electrochimica Acta, 2007, 53(2): 525-537.

[9] Chang J, Lee M, Tsai W, et al. Pseudocapacitive mechanism of manganese oxide in 1-ethyl-3-methylimidazolium thiocyanate ionic liquid electrolyte studied using X-ray photoelectron spectroscopy[J]. Langmuir, 2009, 25 (19): 11955-11960.

[10] Conway B E. Electrochemical supercapacitors: Scientific fundamentals and technological applications[M]. New York: Kluwer Academic/Plenum, 1999.

[11] Zhang Y, Feng H, Wu X, et al. Progress of electrochemical capacitor electrode materials: A review[J]. International Journal of Hydrogen Energy, 2009, 34(11): 4889-4899.

[12] Zhou X H, Peng C, Chen G Z. 20 V stack of aqueous supercapacitors with carbon (-), titanium bipolar plates and CNT-polypyrrole composite (+)[J]. AIChE Journal, 2012, 58(3): 974-983.

[13] Frackowiak E, Khomenko V, Jurewicz K, et al. Supercapacitors based on conducting polymers/nanotubes composites[J]. Journal of Power Sources, 2006, 153(2): 413-418.

[14] Li J P, Peng T Z, Fang C. Screen-printable sol-gel ceramic carbon composite pH sensor with a receptor zeolite [J]. Analytica Chimica Acta, 2002, 455(1): 53-60.

[15] Metters J P, Kadara R O, Banks C E. New directions in screen printed electroanalytical sensors: An overview of recent developments[J]. Analyst, 2011, 136 (6): 1067-1076.

[16] Ji X, Hallam P M, Houssein S M, et al. Printable thin film supercapacitors utilizing single crystal cobalt hydroxide nanosheets [J]. RSC Advances, 2012, 2(4): 1508-1515.

[17] Chen X, Xia J, Peng J, et al. Carbon-nanotube metal-matrix composites prepared by electroless plating [J]. Composites Science and Technology, 2000, 60(2): 301-306.

[18] Hu L B, Choi J W, Yang Y, et al. Highly conductive paper for energy-storage devices [J]. Proceedings of the National Academy of Sciences, 2009, 106(51): 21490-21494.

[19] Hughes M, Chen G Z, Shaffer M S P, et al. Electrochemical capacitance of a nanoporous composite of carbon nanotubes and polypyrrole[J]. Chemistry of Materials, 2002, 14(4): 1610-1613.

[20] Shaffer M S P, Fan X, Windle A H. Dispersion and packing of carbon nanotubes[J]. Carbon, 1998, 36(11): 1603-1612.

[21] Wu M Q, Snook G A, Gupta V, et al. Electrochemical fabrication and capacitance of composite films of carbon nanotubes and polyaniline[J]. Journal of Materials Chemistry, 2005, 15(23): 2297-2303.

[22] Peng C, Zhang S W, Zhou X H, et al. Unequalisation of electrode capacitances for enhanced energy capacity in asymmetrical supercapacitors [J]. Energy & Environmental Science, 2010, 3(10): 1499-1502.

[23] Chae J H, Ng K C, Chen G Z, Nanostructured materials for the construction of asymmetrical supercapacitors [J]. Proceedings of the Institution of Mechanical Engineers, Part A: Journal of Power and Energy, 2010, 224 (A4): 479-503.

[24] Ng K C, Zhang S W, Peng C, et al. Individual and bipolarly stacked asymmetrical aqueous supercapacitors of CNTs/SnO_2 and CNTs/MnO_2 nanocomposites[J]. Journal of The Electrochemical Society, 2009, 156(11): A846-A853.

[25] Hu M, Sui S, Zhu X, et al. A 10 kW class PEM fuel cell stack based on the catalyst-coated membrane (CCM) method [J]. International Journal of Hydrogen Energy, 2006, 31(8): 1010-1018.

[26] Lian K K, Li C, Jung R H, et al (Motorola, Inc.). Electrochemical cell having symmetric inorganic electrodes: United States, WO/1997/015938[P]. 1996.

[27] Staiti P, Lufrano F. Design, fabrication, and evaluation of a 1.5 F and 5 V prototype of solid-state electrochemical supercapacitor [J]. Journal of The Electrochemical Society, 2005, 152(3): A617-A621.

[28] Peng C, Hu D, Chen G Z. Theoretical specific capacitance based on charge storage mechanisms of conducting polymers: Comment on ‘Vertically oriented arrays of polyaniline nanorods and their super electrochemical properties’[J]. Chemical Communications, 2011, 47 (14): 4105-4107.

钛双极片上网印导电聚合物——碳纳米管复合物及其在水型不对称超级电容器中的电化学性能

周晓航, 陈　政*

(诺丁汉大学 工程学部化学工程和环境工程系及能源与可持续性研究所,英国 诺丁汉 NG7 2RD)

摘要: 用导电聚合物(聚吡硌、聚苯胺)与碳纳米管(经酸处理)复合物(ECP-CNT)以及功能添加剂(表面活性剂:苄索氯铵 benzethonium chloride,粘结剂:聚乙烯醇 polyvinyl alcohol)配成水型印泥(aqueous ink),在钛片(厚度:0.1 mm)上网印(screen printing)成所需载量及面积(例如:75 mg·cm^{-2},100 cm^2)的均匀的 ECP-CNT 膜. 以该膜为正极,网印活性炭(pigment black)膜为负极,3.0 mol·L^{-1} KCl 或 1.0 mol·L^{-1} HCl 为电解质,组装不对称超级电容器. 用循环伏安、恒电流充放电、电化学阻抗、光及电显微等方法研究了 ECP-CNT 复合物、网印膜、单池以及由双极片(bipolar plate)连接的多池堆(multi-cell stack). 以两片印刷面积为 100 cm^2 的钛双极片组装成三池堆,得到较好的技术指标:堆电压 3.0 V,电极电容 1.29 ~ 1.83 F·cm^{-2},比能量 2.30 ~ 3.24 Wh·kg^{-1},最大比功率 1.04 kW·kg^{-1}.

关键词: 网印法; 超级电容器; 导电聚合物; 碳纳米管; 双极片; 金属钛